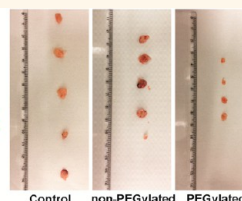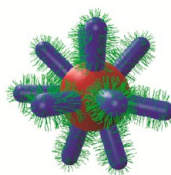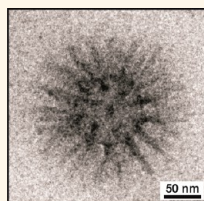# Multicompartment Micelles with Adjustable Poly(ethylene glycol) Shell for Efficient *in Vivo* Photodynamic Therapy

Christopher V. Synatschke,[†] Takahiro Nomoto,[‡] Horacio Cabral,[‡] Melanie Förtsch,[†] Kazuko Toh,[§] Yu Matsumoto,[§,⊥] Kozo Miyazaki,[§] Andreas Hanisch,[†] Felix H. Schacher,[#] Akihiro Kishimura,[‖] Nobuhiro Nishiyama,[▽] Axel H. E. Müller,[†,⊗,*] and Kazunori Kataoka[‡,§,‖,*]

[†]Makromolekulare Chemie II, Universität Bayreuth, D-95440 Bayreuth, Germany, [‡]Department of Bioengineering, Graduate School of Engineering, The University of Tokyo, Tokyo 113-8656, Japan, [§]Division of Clinical Biotechnology, Center for Disease Biology and Integrative Medicine, Graduate School of Medicine, The University of Tokyo, Tokyo 113-0033, Japan, [⊥]Department of Otorhinolaryngology and Head and Neck Surgery, Graduate School of Medicine and Faculty of Medicine, The University of Tokyo, Tokyo 113-8655, Japan, [‖]Department of Materials Engineering, Graduate School of Engineering, The University of Tokyo, Tokyo 113-8656, Japan, [#]Institut für Organische Chemie und Makromolekulare Chemie and Jena Center for Soft Matter (JCSM), Friedrich-Schiller-Universität Jena, D-07743 Jena, Germany, and [▽]Polymer Chemistry Division, Chemical Resources Laboratory, Tokyo Institute of Technology, R1-11, 4259 Nagatsuta, Midori-ku, Yokohama 226-8503, Japan. [⊗]Present address: Institut für Organische Chemie, Johannes Gutenberg-Universität Mainz, D-55099 Mainz, Germany.

ABSTRACT We describe the preparation of well-defined multicompartment micelles from polybutadiene-*block*-poly(1-methyl-2-vinyl pyridinium methyl sulfate)-*block*-poly(methacrylic acid) (BVqMAA) triblock terpolymers and their use as advanced drug delivery systems for photodynamic therapy (PDT). A porphyrazine derivative was incorporated into the hydrophobic core during self-

assembly and served as a model drug and fluorescent probe at the same time. The initial micellar corona is formed by negatively charged PMAA and could be gradually changed to poly(ethylene glycol) (PEG) in a controlled fashion through interpolyelectrolyte complex formation of PMAA with positively charged poly(ethylene glycol)-*block*-poly(L-lysine) (PLL-*b*-PEG) diblock copolymers. At high degrees of PEGylation, a compartmentalized micellar corona was observed, with a stable bottlebrush-on-sphere morphology as demonstrated by cryo-TEM measurements. By *in vitro* cellular experiments, we confirmed that the porphyrazine-loaded micelles were PDT-active against A549 cells. The corona composition strongly influenced their *in vitro* PDT activity, which decreased with increasing PEGylation, correlating with the cellular uptake of the micelles. Also, a PEGylation-dependent influence on the *in vivo* blood circulation and tumor accumulation was found. Fully PEGylated micelles were detected for up to 24 h in the bloodstream and accumulated in solid subcutaneous A549 tumors, while non- or only partially PEGylated micelles were rapidly cleared and did not accumulate in tumor tissue. Efficient tumor growth suppression was shown for fully PEGylated micelles up to 20 days, demonstrating PDT efficacy *in vivo*.

KEYWORDS: polymeric micelles · multicompartment micelles · interpolyelectrolyte complexes · photodynamic therapy · PEGylation

Nanostructured materials are gaining increasing interest for delivering bioactive agents.[1−5] Block copolymers are a highly versatile class of such materials and consequently have been explored for constructing efficient drug delivery systems (DDS) with increasing complexity.[6] Thus, polymeric micelles, which self-assemble from amphiphilic block copolymers are being used for encapsulating drugs and genes in their core, thereby enhancing the availability of the drug in the organism and delivering the incorporated therapeutic molecules to specific tissues.[7−9] Higher degree of sophistication can be provided to block copolymer-based DDS by supplying responsiveness to stimuli, such as pH, salt concentration, magnetic fields or light irradiation, and introducing ligand molecules for specific targeting of disease-related epitopes. Moreover, by combining imaging reporters with block copolymer systems, DDS can be made visible in biological conditions, facilitating the validation of their design. The dual therapeutic and diagnostic function within a single DDS platform, so-called "theranostics", also permits following the therapeutic response and the disease progression.[10−12] Accordingly, smart DDS capable of precisely engineering the loading of agents within their nanostructures may allow the

optimization of both imaging sensitivity and therapeutic efficacy.[13]

In this regard, multicompartment micelles (MCMs) grant the delivery of various active substances simultaneously, by chemically or physically incorporating them in different nanocompartments within the same particle. An elegant approach for the preparation of MCMs is the use of triblock terpolymers, *i.e.*, materials with at least 3 different polymer blocks. Proper choice of a selective solvent for one of the segments allows for the preparation of structures, which are further subdivided in the core or the shell.[14,15] Postpolymerization modification of active groups in MCMs further allows tailoring their properties, such as surface charge or targeting ligands, according to the desired application. For example, the negatively charged corona of core—shell-corona MCMs, prepared from triblock terpolymer polybutadiene-*block*-poly(1-methyl-2-vinyl pyridinium methyl sulfate)-*block*-poly(methacrylic acid) (PB-*b*-P2VPq-*b*-PMAA; BVqMAA), was modified through complexation with the positively charged block of poly-(ethylene glycol)-*block*-poly(2-(dimethylamino)ethyl methacrylate) (PEG-*b*-PDMAEMAq), stabilizing the resulting complex MCMs in water.[16] Despite the clear advantages of MCMs for delivering diagnostic and therapeutic molecules, few examples examining their biological applications can be found in the literature.[17]

In this contribution, we investigated the capability of MCMs prepared from BVqMAA triblock terpolymers as a novel drug delivery platform. BVqMAA micelles present three compartments, *i.e.*, core, shell, and corona, which can serve different functions in the drug delivery process. Thus, as efficient DDS should stably circulate in the bloodstream,[18,19] the properties of the corona of BVqMAA micelles will be important for stabilizing the micelles and avoiding aggregation in biological environments. Two BVqMAA triblock terpolymers, with a long and a short PMAA block, were used as starting material to evaluate the biological properties of the corresponding MCMs (Scheme 1A). Moreover, the effect of the corona composition was investigated by introducing increasing amounts of positively charged poly(ethylene glycol)-*block*-poly(L-lysine) (PLL-*b*-PEG) diblock copolymer to the PMAA corona, which leads to a gradual transition from the negatively charged corona of pure PMAA to the neutral corona of PEG from the same starting MCMs (Scheme 1B). In addition, the ability of BVqMAA micelles for delivering therapeutic molecules to tumor tissues was also considered. Thus, as the core of MCMs serves as a drug reservoir, we incorporated a hydrophobic porphyrazine derivative, which can serve both as a fluorescent probe and a photosensitizer (PS), *i.e.*, a drug that generates reactive oxygen species (ROS) upon light irradiation, for photodynamic therapy (PDT).[20−23] Since the production of ROS in PDT is limited to the site of illumination, the

light-induced cytotoxicity can be spatially controlled to the illuminated area. Nevertheless, because PS distributed to normal tissues, such as skin, causes photosensitivity, patients often have to avoid exposure to sunlight for several weeks. Therefore, promising MCM formulations for PDT treatment of cancer should successfully control the PS bioavailability and enhance the accumulation of the incorporated PS to tumor tissues. Accordingly, detailed studies on the biological properties of these particular MCMs were conducted both *in vitro* and *in vivo* with regard to their ability to function as DDS for PDT.

RESULTS AND DISCUSSION

We prepared PS-carrying polymer micelles from polybutadiene-*block*-poly(2-vinylpyridine)-*block*-poly-(*tert*-butyl methacrylate) (PB-*b*-P2VP-*b*-P*t*BMA; BVT, Scheme 1A, Table S1) analogue to previously published procedures.[16] After quaternization and hydrolysis to BVqMAA, MCMs of well-defined size and structure form spontaneously when the solvent is exchanged to water by dialysis.[24] The hydrophobic porphyrazine derivative, serving as PS, is encapsulated in the PB core of the micelles, while the negatively charged corona from PMAA stabilizes the structures in solution. Two different examples of such micelles, differing in the length of the PMAA block, BVqMAA-1 with a short- (DP$_{PMAA}$ = 400) and BVqMAA-2 with a long corona (DP$_{PMAA}$ = 1350), were prepared in salt containing PBS buffer (10 mM + 140 mM NaCl at pH 7.4) to allow for *in vitro* and *in vivo* experiments. We used two different lengths of PMAA blocks for evaluating the effect of the length of the shell-forming block on the physicochemical and biological properties of the micelles. From potentiometric titration measurements, we determined more than 80% of the MAA groups to be deprotonated at pH 7.4, rendering the BVqMAA micelles strongly negatively charged and thus highly stable under these conditions.

Corona Modification of MCMs. Besides offering the possibility to conjugate functional molecules through esterification, the negatively charged carboxylic acid groups of the PMAA corona can be used for further functionalization through an interpolyelectrolyte complex (IPEC) formation with polycations.[16,25] Here, we integrated a PLL-*b*-PEG (Table S1) diblock copolymer, as illustrated in Scheme 1B, simply by complexing PLL-*b*-PEG with long- and short corona BVqMAA micelles. The complexation ratio is given as $Z_{+/-}$-value, which is defined as the ratio between cationic lysine monomer units divided by the residual number of anionic MAA monomer units after taking the intramicellar IPEC with Vq into account (see eq 1).

$$Z_{+/-} = \frac{n_{Lys}}{n_{MAA} - n_{Vq}} \tag{1}$$

This allows us to gradually change the corona composition from a pure PMAA corona for noncomplexed
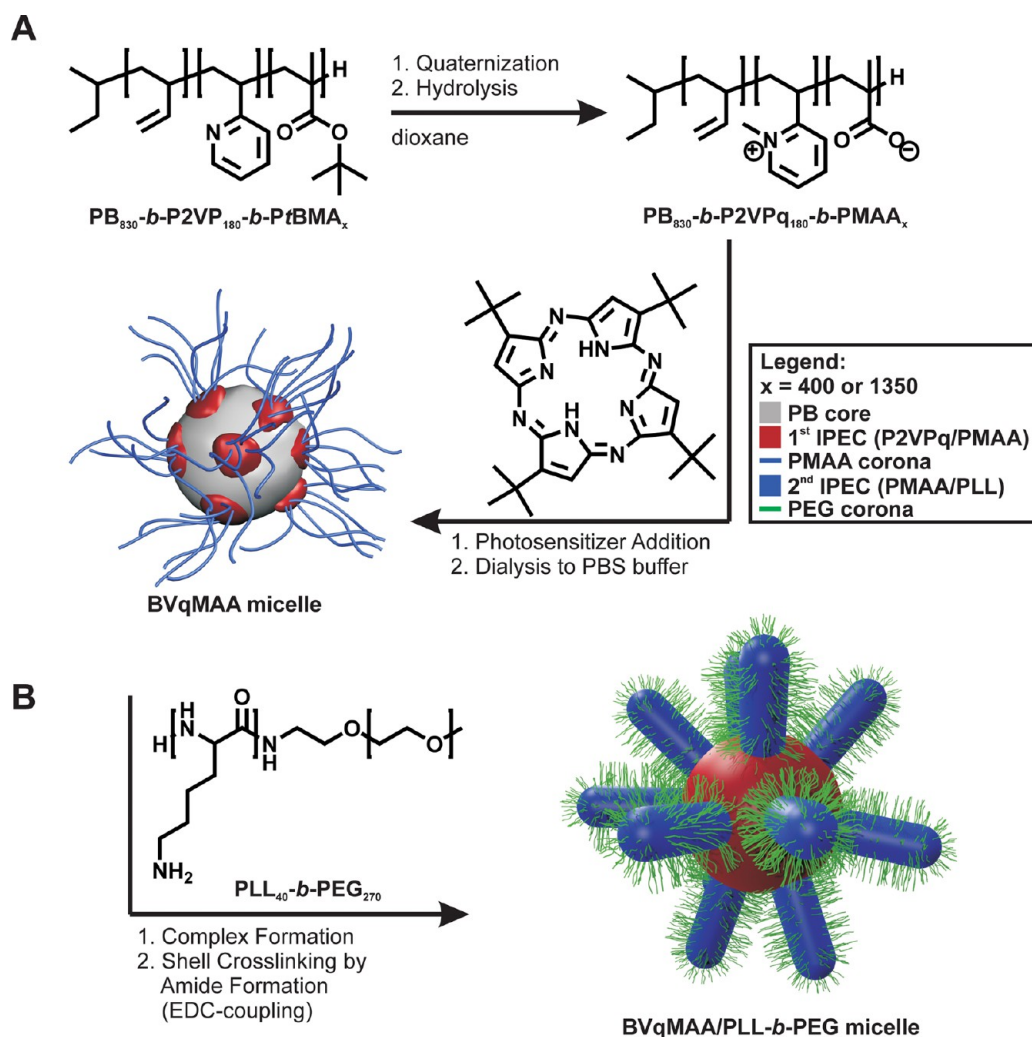
Scheme 1. (A) Preparative procedure to obtain PS-carrying BVqMAA micelles in water. A BVT triblock terpolymer is quaternized and hydrolyzed in dioxane to give amphiphilic BVqMAA. After PS addition, self-assembly to micelles takes place through the exchange of solvent from dioxane to PBS buffer. (B) Complexation with PLL-*b*-PEG diblock copolymers and subsequent crosslinking of PMAA with PLL yields PEGylated micelles (BVqMAA/PLL-*b*-PEG).

micelles ($Z_{+/-} = 0$) to a complete PEG corona for micelles where all PMAA has been complexed with PLL to form an IPEC ($Z_{+/-} = 1$). Complexation ratios in between these two cases give partially PEGylated micelles. For each corona-length of the BVqMAA micelles, four ratios with PLL-*b*-PEG were prepared ($Z_{+/-} = 0$; 0.25; 0.5 and 1). To prevent any dissociation of the IPEC in biological surroundings, the lysine and MAA units were cross-linked with 1-ethyl-3-(3-dimethylaminopropyl) carbodiimide hydrochloride (EDC-coupling). The characterization of the resulting micelles by ζ-potential measurements and dynamic light scattering (DLS) as well as the determination of the corresponding mass and PS concentration is summarized in Table 1.

The mass loading of BVqMAA/PLL-*b*-PEG micelles with PS is between 6 and 12%. The ζ-potential values of the non-PEGylated micelles were strongly negative, as was expected for the deprotonated PMAA corona at pH 7.4. With increasing complexation ratio, these values (after cross-linking) increased and reached almost zero

at $Z_{+/-} = 1$, suggesting successful complex formation and surface coverage by PEG. The cumulant hydrodynamic diameter, D_h, of the micelles varied between 260 and 290 nm, but no significant correlation between complexation ratio and micellar size was observed. During IPEC formation, two opposing effects might simultaneously influence the size of the micelles. That is, through binding of the PMAA corona and its subsequent collapse to form the IPEC, the size of the micelles decreases, while the introduction of uncharged PEG into the corona increases micelle size. All the micelles show narrow D_h distributions with dispersities, D.I., between 0.026 and 0.073 and the core size of BVqMAA-1 and BVqMAA-2 remains essentially unchanged by PEGylation (Table S2).

The structure of BVqMAA/PLL-*b*-PEG micelles was investigated by cryogenic transmission electron microscopy (cryo-TEM) measurements, where the micellar structure can be imaged close to its native state in aqueous solution. The top row of Figure 1 shows representative

images from the BVqMAA-1/PLL-*b*-PEG micelles in PBS buffer solution with increasing amount of PLL-*b*-PEG used for complexation from left to right. In the bottom row, the corresponding structures from BVqMAA-2 are depicted. An overview of the sample is provided in each image, including the average D_h from light scattering measurements represented as a circle, while a single enlarged micelle is shown in the inset.

For the noncomplexed BVqMAA-1 ($Z_{+/-} = 0$) micelles, a core−shell-corona structure was evident from the dark gray ring (intramicellar IPEC between P2VPq and PMAA) surrounding the gray PB core. Water swells the PMAA corona of the micelles and consequently reduces the electron contrast, making it hard to distinguish from the surrounding water phase. As expected from theory,[26] the core-size of the BVqMAA-1/PLL-*b*-PEG

TABLE 1. Characterization of BVqMAA-1 and BVqMAA-2 Micelles with Increasing Degree of PEGylation with Regard to Polymer and Photosensitizer (PS) Concentration, ζ-Potential and Cumulant Hydrodynamic Diameter with Corresponding Dispersity Index (D.I.)[a]

polymer	$Z_{+/-}$-value	mass conc. [g/L][b]	PS conc. [μM][c]	ζ-potential [mV]	D_h [nm]	D.I.
BVqMAA-1	0	0.47	106	−28	259	0.043
	0.25	0.60	105	−7.5	262	0.043
	0.5	0.52	97	−4.0	264	0.049
	1	0.91	117	−0.2	286	0.059
BVqMAA-2	0	0.88	130	−31	287	0.052
	0.25	0.62	140	−13	280	0.073
	0.5	1.10	140	−6	255	0.026
	1	1.52	165	−2	280	0.028

[a] All micelle solutions were in 10 mM PBS buffer solution at pH 7.4 with additional 140 mM NaCl. [b] Concentration of drug carrying polymer micelles determined by weight after freeze-drying of aliquot dialyzed to Milli-Q water to remove buffer salts. [c] Determined from absorbance at 552 and 620 nm of freeze-dried aliquot redissolved in DMAc.

micelles was larger than that of the corresponding BVqMAA-2/PLL-*b*-PEG micelles (Table S2), due to a decreased aggregation number for longer PMAA chains in BVqMAA-2. Upon addition of PLL-*b*-PEG, the structure of the micelles gradually changed. At a low $Z_{+/-}$-value of 0.25, the density of the corona increased and an enhanced contrast was observed in the cryo-TEM images, indicating a successful complex formation. However, when further PLL-*b*-PEG was added ($Z_{+/-} = 0.5$), the formation of a distinct IPEC structure occurred within the corona. Ray-like structures of high electron density appeared perpendicular to the micellar core, alternating with areas of lower electron density. At a $Z_{+/-}$-value of 1, the segregation of the corona was most prominent for both micelles and the length of the individual rays slightly increased as compared to $Z_{+/-} = 0.5$. Interestingly, the length of the ray-like structures is considerably longer for BVqMAA-2, which is probably a result of its longer PMAA block as compared to BVqMAA-1. Generally, the cumulant hydrodynamic diameters measured for each sample by DLS agree well with the size of the micelles found in cryo-TEM. Only for BVqMAA-2 samples at low complexation ratio, the micelles seem to pack closer than would be expected according to their size observed in light scattering experiments. However, this might originate from confinement effects during cryo-TEM sample preparation. Presumably, the dark rays consist of newly formed IPEC between PMAA and PLL, while the areas of low electron contrast can be attributed to water swollen PEG surrounding these IPEC domains; thus, this might be regarded as a "bottlebrush-on-sphere morphology". Similar structures were previously observed exclusively as a transitional state within the first hours after mixing BVqMAA micelles with PEG-*b*-P2VPq diblock copolymers,[25] finally settling for a layered arrangement of the additional IPEC in an onion-type structure as was also found
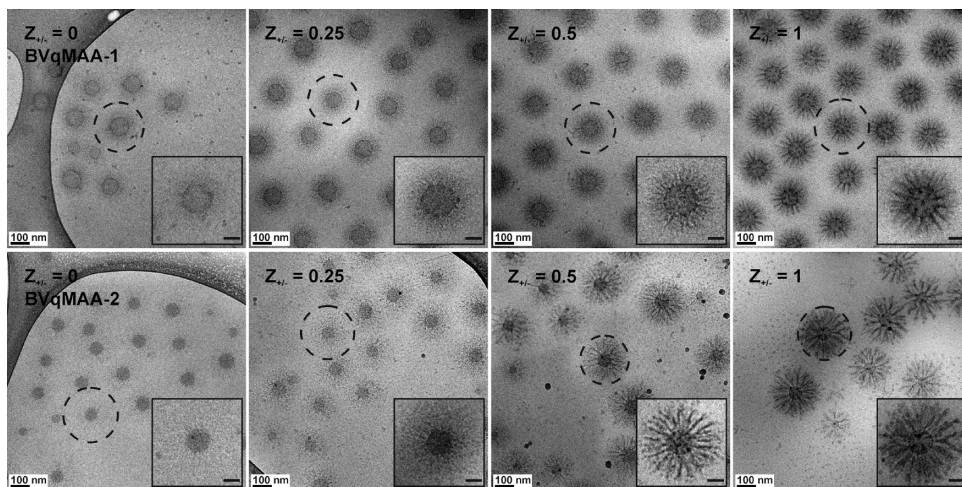

Figure 1. Cryo-TEM micrographs of BVqMAA micelles after complex formation with increasing amounts of PLL-*b*-PEG and subsequent cross-linking by EDC-coupling (scale bar = 100 nm). Top row, BVqMAA-1; bottom row, BVqMAA-2 micelles. The circle represents the average D_h of the respective sample determined by light scattering. The inset in each micrograph shows a single enlarged micelle from each batch with the scale bar representing 50 nm.

for PEG-*b*-PDMAEMAq as block copolymer with a polycationic segment.[16] However, in the current case, the observed structures remained unchanged for months. One possible reason for the peculiar morphology may be the secondary structure of PLL. Homopolymers of PLL are known to form intramolecular hydrogen bonds in their uncharged state, leading to the formation of α-helical secondary structures.[27] Indeed, CD-spectroscopy measurements as depicted in Figure S1 of the complex micelles confirmed the existence of α-helical structures, even after cross-linking, which were absent in solutions of noncomplexed BVqMAA micelles in the same buffer, respectively. To clarify whether the secondary structure of PLL is indeed responsible for the peculiar morphology of the micellar corona, we synthesized a poly(D,L-lysine)-*block*-poly(ethylene glycol) (PDLL-*b*-PEG) diblock copolymer with similar block lengths, which cannot form α-helices (Table S1). As expected, the CD-spectra indicated the absence of secondary structures (Figure S1) for BVqMAA micelles after complex formation with PDLL-*b*-PEG. Nevertheless, comparable morphologies were found for BVqMAA/PDLL-*b*-PEG complexes (Figure S2), leading to the assumption that the secondary structure formation of PLL is not responsible for the observed micellar morphology.

Another possible reason for the formation of the bottlebrush-on-sphere morphology is the block length ratio between PMAA and PLL. The positively charged lysine block has a rather short DP of 40 units (due to synthetic constraints on controlled block lengths of PLL), while the PMAA chain of the BVqMAA polymers even after intramolecular IPEC formation with P2VPq retains a length of 220 and 1170 theoretically accessible units for BVqMAA-1 and BVqMAA-2, respectively. Consequently, for full compensation of the negative charges of a single PMAA chain 5.5 and 29 PLL-*b*-PEG chains are necessary on average for the short and long MAA blocks, respectively. To accommodate these large amounts of PLL-*b*-PEG diblock copolymer within the micelle corona, the system may adopt the observed bottlebrush morphology. With such a conformation, the PLL segments of PLL-*b*-PEG copolymers can reach the MAA units of the corona chains, forming interpolyelectrolyte complexes in the core of the bottlebrushes and segregating the PEG chains. In previous complexation experiments with polycation-*block*-PEG diblock copolymers,[16,25] the polycations were longer than in the current case and consequently a smaller amount of complexing polymer needed to be incorporated into the micelle corona eliminating the need for corona phase separation. The secondary structure and reduced chain flexibility of the PLL might further promote the formation of the observed structures.

Stability of Complex Micelles. IPEC formation is a reversible process and is driven by the gain in translational entropy upon release of low molecular weight counterions as well as electrostatic attraction between oppositely charged monomer units within the polyelectrolyte chains.[28] Therefore, an exchange of polyelectrolytes bound in the IPEC with competing polyions from the surrounding solution can occur under certain conditions, *i.e.*, when the polyelectrolyte chains within the complex are mobile. At high salt concentrations (typically 0.5−1 M) in the media, the charge attraction between polyelectrolytes is weakened and the IPEC is prone to even complete dissolution. Although such extreme salt concentrations do not occur in cell-culture medium or the blood, the presence of serum proteins combined with an increasing dilution of the BVqMAA/PLL-*b*-PEG micelles may lead to polyion exchange reactions, thereby changing the corona composition. To prevent any significant change after complex formation, lysine and methacrylic acid units were covalently cross-linked *via* amide bonds by EDC-coupling. The high stability of the resulting cross-linked micelles is shown in Figure 2, where the structures at original buffer conditions (10 mM PBS buffer at pH 7.4 with 140 mM NaCl) are compared to those at high ionic strength (10 mM PBS buffer at pH 7.4 with 990 mM NaCl), simulating highly challenging conditions in biological media.

As can be seen from the top row images in Figure 2, at low salt concentration there is no significant structural difference between the BVqMAA-2/PLL-*b*-PEG micelles at a $Z_{+/-}$-value of 1, before and after cross-linking, since both samples exhibit the previously discussed bottlebrush-on-sphere morphology. Upon increasing the salt concentration of the buffer from 140 mM to 990 mM NaCl, the corona of the original, noncomplexed BVqMAA-2 micelles (bottom left image, Figure 2) collapsed due to charge screening. Also, the noncrosslinked and complexed micelles showed a collapse of the corona accompanied by a loss of the bottlebrush morphology, suggesting a partial dissolution of the IPEC domains. In contrast, the bottlebrush morphology is retained for cross-linked BVqMAA-2/PLL-*b*-PEG, even at high ionic strength of the solution. Since the crosslinked micelles showed a high tolerance against challenging solvent conditions, we expect the micelles to remain structurally intact and prevent polyion exchange reactions in biological surroundings.

Biological Characterization. Next, the biological properties of the BVqMAA micelles and their complexes with PLL-*b*-PEG were investigated. As a model drug, a hydrophobic porphyrazine derivative was incorporated into the micellar core during micelle formation. This general class of molecules has previously been used as photosensitizer (PS), creating reactive oxygen species (ROS) upon photoirradiation.[29] To test the capacity of the micelles for drug delivery, we evaluated the *in vitro* cytotoxicity and cellular uptake of the PS-loaded MCMs. Cellular toxicity was tested against A549 human lung cancer cells, which were treated with increasing concentrations of PS-carrying micelles
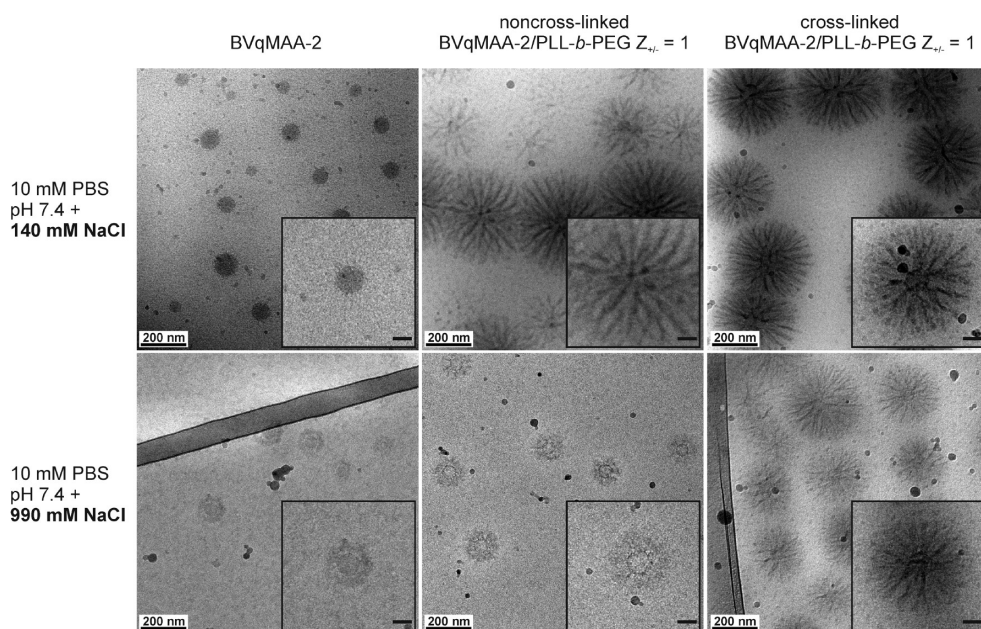
Figure 2. Micelle stability against challenging solvent conditions. Representative cryo-TEM micrographs of BVqMAA-2/PLL-*b*-PEG complex micelles in buffer solution at low (top row) and high (bottom row) ionic strength. Left column images show pure BVqMAA-2 micelles, while middle and right column images depict the complexes with PLL-*b*-PEG ($Z_{+/-}$ = 1) before and after cross-linking, respectively. Scale bars in each micrograph represent 200 nm. The inset in each micrograph shows a single enlarged micelle in more detail with the scale bar representing 50 nm.

TABLE 2. *In Vitro* PDT Efficacy. IC$_{50}$ Values (μg PS/mL Medium) of BVqMAA/PLL-*b*-PEG Micelles Carrying PS against A549 Cells in Dependence of the Degree of PEGylation and Illumination Time (0, 15, and 30 min) as Determined by MTT Assay

	BVqMAA-1/PLL-*b*-PEG			BVqMAA-2/PLL-*b*-PEG		
$Z_{+/-}$-value	0 min	15 min	30 min	0 min	15 min	30 min
0	9.3	0.07	0.04	8	<0.02	<0.02
0.25	>10	0.13	0.05	>10	0.12	0.07
0.5	>10	0.21	0.08	>10	0.22	0.26
1	>10	0.77	0.28	>10	0.13	0.54

Figure 3. *In vitro* cellular uptake. Amount of PS per 10^6 A549 cells in dependence of the $Z_{+/-}$-value of BVqMAA/PLL-*b*-PEG micelles after an incubation time of 24 h (*n* = 3).

followed by photoirradiation. From the relative viability data, we determined an inhibitory concentration for 50% of the cells (IC$_{50}$), which is summarized in Table 2 for different photoirradiation times, $Z_{+/-}$-values and both micelle types.

In the control samples without a photoirradiation step (0 min), all the micelles had IC$_{50}$-values above or close to the maximum tested PS concentration of 10 μg/mL; IC$_{50}$-values drastically decreased upon illumination. Generally, a prolonged illumination resulted in an increased cytotoxicity (lower IC$_{50}$ values), as would be expected for a continuous ROS production leading to increasing cellular damage. Since PS-unloaded micelles (Table S3) were not cytotoxic against these cells (Table S4), the cytotoxicity observed for PS-carrying micelles upon irradiation should be a result of the ROS production from the PS. Interestingly, we found a strong influence of the PEGylation degree of the
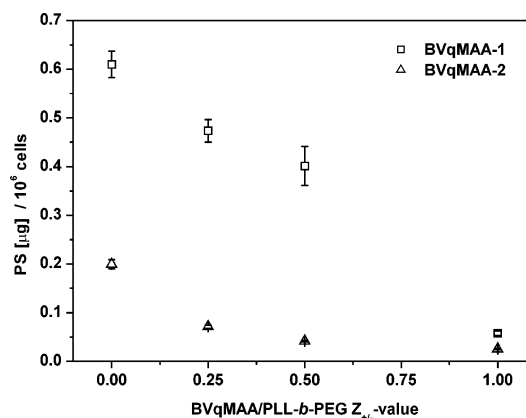
micelles on cytotoxicity, with illuminated non-PEGylated micelles exhibiting the lowest IC$_{50}$-values of all samples. The cytotoxicity of both micelle types (BVqMAA-1 and 2) decreased with increasing $Z_{+/-}$-value. The uptake behavior of the micelles could explain this observation (Figure 3). There, a strong dependence of the cellular uptake with the micelle corona composition was also found. Interestingly, even though BVqMAA-1/PLL-*b*-PEG micelles exhibited high cell uptake of PS (especially for low $Z_{+/-}$ values), they failed to show strong photoinduced cytotoxicity, probably because ROS production from PS-loaded BVqMAA-1/PLL-*b*-PEG micelles was not as efficient as from PS-loaded BVqMAA-2/PLL-*b*-PEG micelles. The difference in the corona composition of the micelles may

affect their interaction with both the surface of cells and the serum molecules in the medium. Thus, strongly charged colloidal objects, such as the micelles with a low degree of PEGylation, should strongly interact with proteins in the serum as well as the cell surface, resulting in enhanced cellular uptake. At the same time, micelles with near complete PEGylation have a nearly neutral ζ-potential in combination with a steric shielding effect from the PEG chains in the corona. Both effects should consequently decrease the interaction of the micelles with the cellular membrane, thereby decreasing cellular uptake.[30] In *in vitro* stability experiments, we found that the micelles remain stable in serum-containing cell culture media for at least 24 h, as only minor changes in the hydrodynamic radius of the micelles and the absence of large aggregates were observed (Figure S3). In the measurement, protein adsorption could be masked to a certain extent through a simultaneous collapse of the corona. However, since most proteins in the cell culturing medium are also negatively charged we assume protein adsorption to occur only to a minor extent, at least *in vitro*.

Since an increased blood circulation leads to an improved accumulation of nanosized carriers in tumors due to highly permeable blood vessels and immature lymphatic systems, which is the so-called enhanced permeation and retention (EPR) effect,[31] the surface modification of the micelles is expected to affect the blood circulation time and eventual accumulation in tumor tissue. We therefore evaluated the blood circulation of different BVqMAA/PLL-*b*-PEG micelles using intravital real-time confocal laser scanning microscopy (IVRTCLSM), which permits *in situ* monitoring and semiquantitative analysis of fluorescence-labeled DDS.[32] We intravenously injected both types of micelles (BVqMAA-1 and BVqMAA-2) with varying degrees of PEGylation to female Balb/c nu/nu mice, and observed the fluorescence of the PS in the earlobe vein to quantify the blood circulation (Figure 4A,B). Original fluorescence images shortly after injection and at 60 min circulation time are depicted in Figure S4. As with the *in vitro* cellular uptake study, we found a strong dependence of the blood circulation time on the degree of PEGylation. Only fully PEGylated micelles had a prolonged plasma circulation of several hours: >20% for BVqMAA-1/PLL-*b*-PEG and >30% for BVqMAA-2/PLL-*b*-PEG at 2 h. All other micelles, which were partially or non-PEGylated, reached less than 10% in 15 min, indicating a fast clearance from the bloodstream. These results indicate an improvement of the circulation properties with increasing degree of PEGylation, as would be expected from the increased shielding effect of PEG and simultaneous reduction of charge density. Accordingly, long PEG chains and a high packing density are necessary to reduce protein adsorption on the surface of nanoparticles and extend their blood circulation, with the density being more

significant than the length of the polymer. However, increasing density of PEG chains in the corona reduces chain mobility and flexibility, which in turn leads to less protein adsorption due to steric hindrance.[30,33] A correlation between better blood circulation and increased PEG density was recently shown for rod-like polymeric micelles from plasmid DNA complexed with different PLL-*b*-PEG diblock copolymers.[34] There, micelles with improved blood circulation properties had a "squeezed" PEG conformation, which impedes opsonization and subsequent clearance. Thus, when comparing the circulation times of the two fully PEGylated micelles, BVqMAA-2/PLL-*b*-PEG showed higher amounts in the plasma, with roughly 10% of relative fluorescence intensity after 2 h, probably due to the larger amount of PLL-*b*-PEG necessary to reach complete compensation of the long MAA corona, *i.e.*, high PEG-density. Moreover, the circulation time observed for BVqMAA/PLL-*b*-PEG micelles is in between that reported for different PEGylated polymersomes of similar size. While PICsomes with a size of 256 nm had a much longer circulation time ($T_{1/2}$ = 9.7 h),[35] polymersomes from a PB-*b*-PEG diblock copolymer[36] were cleared more rapidly than BVqMAA/PLL-*b*-PEG micelles. Apart from the circulation time it is rather difficult to compare the herein demonstrated BVqMAA/PLL-*b*-PEG micelles with other systems as they are larger than most polymeric micelles and, while similar in size, the mechanical properties compared to polymersomes might differ significantly. Additionally, the surface topology resulting from the "bottlebrush-on-sphere" morphology might have an influence on the interaction with biological media.

To get more insight about the *in vivo* activity of the micelles, we evaluated the biodistribution of the micelles in mice bearing subcutaneous A549 tumors (Figure 4C and supporting Figure S5). As can be seen in Figure 4C, the partially or non-PEGylated micelles could not deliver the PS to the tumor site and only fully PEGylated micelles showed high accumulation of the drug at approximately 4% of the injected dose in the tumors. These findings correlate with the prolonged circulation times of PEGylated micelles and indicate the tumor targeting of these micelles by EPR effect. Also, it is well-known that nanoparticles larger than 200 nm are likely to be entrapped in liver and spleen.[35−38] Indeed, the BVqMAA/PLL-*b*-PEG micelles were mainly cleared by spleen and liver (Figure S5). The tumor targeting with the micelles might be further improved by decreasing their size below 200 nm.

The prolonged blood circulation and eventual enhanced tumor accumulation of fully PEGylated micelles led to efficient PDT treatment. We evaluated the PDT efficacy of BVqMAA-2/PLL-*b*-PEG micelles with $Z_{+/-}$ = 1 against subcutaneous A549 tumors. Non-PEGylated BVqMAA-2 micelles and nontreated mice served as control. Twenty-four h after the injection, the mice were illuminated at the tumor site with a xenon
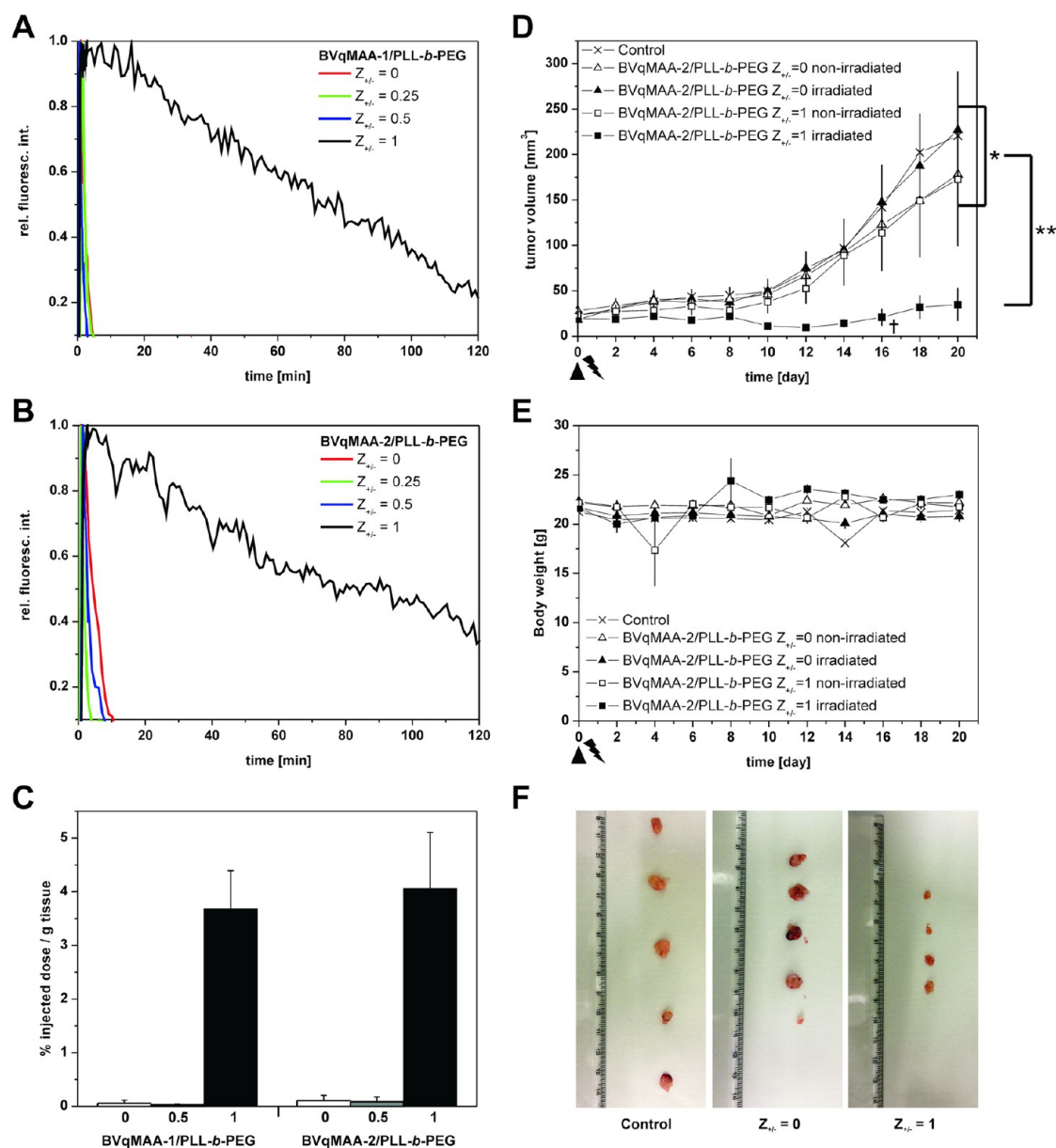
Figure 4. *In vivo* circulation time of PS-carrying BVqMAA-1 (A) and BVqMAA-2 (B) micelles with increasing degree of PEGylation in female Balb/c nu/nu mice. (C) Accumulation of PS in subcutaneous A549 tumor model 24 h after injection of BVqMAA/PLL-*b*-PEG $Z_{+/-} = 1$ micelles ($n = 4$). *In vivo* PDT efficacy study ($n = 5$). Evolution of the tumor volume (D) and body weight (E) with time. †: 1/5 tumor regression. *$p > 0.05$; **$p < 0.001$. (F) Comparison of tumor sizes resected 21 days after BVqMAA-2/PLL-*b*-PEG injection and laser treatment.

lamp equipped with a 630 nm long-path filter to induce ROS production. The evolution of the tumor volume was monitored for 20 days as shown in Figure 4D. Only fully PEGylated micelles combined with photoirradiation significantly inhibited the tumor growth, even leading to complete tumor regression in one mouse, while the non-PEGylated micelles after irradiation exhibited a negligible antitumor activity (Figure 4D,F). Also, we found no significant change in the body weight (Figure 4E) throughout the whole study, suggesting a negligible toxicity of the micelles. Intense necrosis was observed at the tumor site (Figure S6) for fully PEGylated micelles after photoirradiation,

indicating successful ROS production. The necrosis might have induced an activation of the immune system, further aiding in tumor regression in addition to cellular damage from ROS. These findings clearly demonstrate the effective treatment of A549 tumors by modifying the corona of the micelles and the overall capacity of the BVqMAA/PLL-*b*-PEG micelles to successfully act as DDS.

CONCLUSIONS

BVqMAA triblock terpolymer micelles were shown to be effective delivery vehicles for a hydrophobic model drug, which proved to be efficient in PDT treatment of

A549 lung-cancer cells both *in vitro* and *in vivo*. By changing the corona composition from a highly negatively charged PMAA to neutral PEG in a controlled manner, we demonstrated the strong influence of the micellar corona on the interaction with biological systems, as is evident by differences in cellular uptake, blood circulation properties and PDT efficacy. The PMAA length of the underlying BVqMAA micelles was of minor importance for the biological properties of the micelles. In principle, any water-soluble block copolymer with a positively charged segment can be used for the corona modification, thereby offering a tool to produce micelles with versatile corona functionalities. Specific targeting molecules could be easily introduced through this mechanism. It remains to be seen whether the observed "bottlebrush-on-sphere" morphology can have a beneficial influence, for example, in cellular recognition. Future work is being directed at exploring the full potential of the different compartments of this advanced carrier system.

EXPERIMENTAL SECTION

Materials. For anionic polymerization THF (Sigma-Aldrich, *p.a.* quality) was first distilled over CaH_2 followed by a distillation over potassium and stored under N_2 before use. Butadiene (Rießner-Gase, 2.5) was purified by passing through columns filled with molecular sieves (4 Å) and basic aluminum oxide, before condensation into a glass reactor and storage over dibutylmagnesium. 2-Vinylpyridine (97%, Aldrich) was deinhibited by passing through a basic aluminum oxide column, subsequently stirred for 30 min with 2 mL of trioctylaluminium per 10 mL of 2-vinylpyridine and finally condensed to a sealable glass ampule under reduced pressure. *tert*-Butyl methacrylate (*t*BMA, 98%, Aldrich) was stirred with 0.5 mL of trioctylaluminium per 10 mL of *t*BMA for 30 min and then condensed to a sealable ampule under reduced pressure. 1,1-Diphenylethylene (DPE, Aldrich, 97%) was stirred with *sec*-butyllithium (*sec*-BuLi) under N_2 and then distilled. *sec*-BuLi (Aldrich, 1.4 M in cyclohexane), dibutylmagnesium (Aldrich, 1 M in heptane) and trioctylaluminum (Aldrich, 25 wt % in hexane) were used as received. Quaternization of 2-vinylpyridine was performed with dimethyl sulfate (Me$_2$SO$_4$, >99%, Aldrich) and used without further purification. For hydrolysis of P*t*BMA to PMAA, conc. HCl (32%, 1.2 g/L, Sigma-Aldrich) was used as received. NCA-L-Lys(TFA) and NCA-DLys(TFA) monomers were prepared by the Fuchs-Farthing method using triphosgene.[39] α-Methoxy-ω-amino-PEG (PEG-NH$_2$, M_n = 12 000 g/mol, PDI = 1.03) was purchased from NOF Corporation (Tokyo, Japan). DMF (*p.a.* quality, TCI) was stored over molecular sieves (4 Å) and subsequently distilled under vacuum and was stored under argon atmosphere before use. Methanol, dioxane (*p.a.* quality, TCI), *N,N*-dimethylacetamide (DMAc, *p.a.* quality, TCI) DMSO-d_6, D$_2$O (both Sigma-Aldrich) and CDCl$_3$ (Deutero, Kastellaun, Germany) were used without further purification. The porphyrazine derivate 2,7,12,17-tetra-*tert*-butyl-5,10,15,20-tetraaza-21*H*,23*H*-porphine (dye content 85%, Sigma-Aldrich) and *N*-(3-dimethylaminopropyl)-*N'*-ethylcarbodiimide hydrochloride (EDC, Sigma-Aldrich) were used as received. Sterile Millex AA syringe filters (0.8 μm, mixed cellulose esters) were delivered from Millipore. Milli-Q water purified with a Millipore filtering system was used in all cases. For dialysis, membranes made from regenerated cellulose (Spectrum Laboratories, Spectra/Por MWCO 1, 3.5, 6−8, and 12−14 kDa) were used.

Synthesis of Polybutadiene-*block*-poly(2-vinylpyridine)-*block*-poly(*tert*-butyl methacrylate) (BVT) Triblock Terpolymers. Sequential living anionic polymerization with *sec*-BuLi as initiator and THF as solvent in a laboratory autoclave (2.5 L) at low temperatures was used for the synthesis of BVT triblock terpolymers. The procedure was carried out analogue to our previously published procedures.[40,41] During the polymerization of the *tert*-butyl methacrylate (*t*BMA) block, samples were withdrawn at different conversions, thereby creating triblock terpolymers varying only in the block length of their final block, while both previous blocks are of the same length. In detail, 1.6 L of dry THF were placed in a 2.5 L laboratory autoclave (Büchi) and titrated at −20 °C with 16 mL of *sec*-BuLi solution (1.4 M in hexane) to remove any protic species that may terminate the polymerization and left to warm to room temperature overnight. The so-formed alkoxides exhibit stabilizing effects on the living chain

end and in the case of *t*BMA well-defined polymers are accessible without addition of LiCl.[42] After the reaction solution was cooled to −70 °C, 0.69 mL of *sec*-BuLi (1 equiv, 9.66 $\times$ 10^{-4} mol) was added, followed by the addition of 63.5 mL of butadiene (41.91 g, 800 equiv, 0.7748 mol) and polymerization for 8 h at −25 °C and further 2 h at −10 °C. 2-Vinylpyridine (21.68 g, 210 equiv, 0.2062 mol) was added at −70 °C and stirred for 2 h, before 0.85 mL of DPE (5 equiv, 4.815 $\times$ 10^{-3} mol) was injected and the solution stirred for 2.5 h at −50 °C. Then, at −70 °C, 167.9 g of *t*BMA (1200 equiv, 1.181 mol) was added to the solution, which led to an immediate rise in the temperature to −60 °C. The reaction temperature was increased to −50 °C and approximately 1/3 of the reaction solution was withdrawn and quenched in degassed isopropanol (200 mL) after 40 min, 2 and 8 h of reaction time, respectively. The final polymer was obtained after precipitation from THF solution containing butylated hydroxytoluene (BHT) as stabilizer into a 1/1 mixture of methanol and H$_2$O. The degrees of polymerization of each block were calculated from a combination of MALDI-ToF-MS of the polybutadiene block and ^{1}H NMR of the final triblock terpolymer and determined to be B$_{830}$V$_{180}$T$_{400}$ and B$_{830}$V$_{180}$T$_{1350}$ for the two polymers used in this work, respectively. Size exclusion chromatography of the two polymers showed bimodal distributions in the elution curves of both polymers, which come from a small amount of terminated PB-*b*-P2VP diblock copolymer during the injection of *t*BMA monomer. The polydispersity indices (PDI) of the full sample were determined to be 1.04 and 1.08 for B$_{830}$V$_{180}$T$_{400}$ and B$_{830}$V$_{180}$T$_{1350}$, respectively.

Synthesis of Polylysine-*block*-poly(ethylene glycol) (PLL-*b*-PEG and PDLL-*b*-PEG). For the synthesis of PLL-*b*-PEG, 1.059 g of *N*-carboxy anhydride of the trifluoroacetyl protected L-lysine (NCA-L-Lys-(TFA), 3.949 mmol, 45 equiv) was placed under argon atmosphere in a 50 mL round-bottom-flask equipped with a magnetic stirrer bar, which had previously been evacuated overnight and were dissolved in 7 mL of dry DMF (containing 1 M thiourea). To this solution, 1.053 g of α-methoxy-ω-amino PEG (PEG-NH$_2$, 8.775 $\times$ 10^{-2} mmol, 1 equiv) with a number average molecular weight of 12 000 g/mol (PDI = 1.03) and dissolved in 1 mL of dry DMF (1 M thiourea) was added under argon atmosphere to serve as macroinitiator. The mixture was allowed to polymerize at 25 °C for 72 h until all monomer had been consumed as observed by IR spectroscopy (signals at 1850, 1760, and 915 cm^{-1} disappear). The block copolymer was purified by dialysis against methanol (Spectra/Por membrane from regenerated cellulose with MWCO = 3500 Da) for 2 d with repeated exchange of dialysis solution. Methanol was evaporated and the pure polymer (1.84 g, 95% yield) was obtained after freeze-drying from dioxane. ^{1}H NMR gave a degree of polymerization of 40 for the TFA-protected L-Lysine and SEC with DMF as eluent and PEG as calibration standard an apparent molecular weight of $M_{n,app.}$ = 22 100 g/mol with a PDI of 1.05. Deprotection was achieved by dissolving 1 g of PLL(TFA)-*b*-PEG in 100 mL of methanol mixed with 10 mL of 5 M NaOH solution and stirring in an open flask at 35 °C for 10 h. The deprotected PLL-*b*-PEG diblock copolymer was purified by dialysis against pH 4 aqueous solution (Spectra/Por membrane from regenerated cellulose with MWCO = 1 kDa) and obtained as a white powder after freeze-drying (800 mg, 86% yield). ^{1}H NMR (Figure S7)

showed full deprotection and unchanged degree of polymerization for the lysine block, giving PLL$_{40}$-b-PEG$_{270}$, where the subscripts denote the respective degrees of polymerization.

The synthesis of PDLL-b-PEG was achieved analogue to the procedure for PLL-b-PEG, except for using a 1/1 mixture between NCA-D-Lys(TFA) and NCA-L-Lys(TFA) as monomers. A 96% yield was obtained for the trifluoroacetyl-protected diblock copolymer PDLL(TFA)-b-PEG after purification, where ^{1}H NMR showed a DP of 38 for the PDLL(TFA) block and SEC measurements with DMF as eluent gave $M_{n,app.} = 24\,800$ g/mol with the PDI = 1.03. The yield of PDLL$_{38}$-b-PEG$_{270}$ after complete deprotection and purification was 58%.

Synthesis of Polybutadiene-*block*-poly(1-methyl-2-vinyl pyridinium methyl sulfate)-*block*-poly(methacrylic acid) (BVqMAA) Triblock Terpolymer Micelles. In a typical reaction, 50 mg of B$_{830}$V$_{180}$T$_{400}$ (4.14×10^{-7} mol) was dissolved in 15 mL of dioxane (*p.a.* quality) in a round-bottom-flask equipped with a magnetic stirrer bar. After addition of 0.94 g of Me$_2$SO$_4$ (0.71 mL, 7.45×10^{-3} mol, 100 equiv compared to 2-vinylpyridine units), the flask was sealed and stirred for 5 d at 40 °C. Subsequently, 1.89 g of conc. HCl solution (1.57 mL, 1.65×10^{-2} mol, 100 equiv compared to tBMA units) was added and the mixture was refluxed at 110 °C for 24 h. For the preparation of PS-containing micelles, 5.39 mg of porphyrazine derivate (1×10^{-5} mol) was dissolved in the mixture at ambient temperature. Self-assembly to B$_{830}$Vq$_{180}$MAA$_{400}$ micelles was achieved through dialysis of the mixture first to 0.1 N NaOH solution (3 d with regular exchange of the dialysis solution, MWCO = 6−8 kDa) and finally dialysis to 10 mM PBS solution at pH 7.4 containing 140 mM NaCl for another 3 d. After dialysis was completed, part of the micelle solution was directly used for complex formation with PLL-b-PEG as described below. In the case of B$_{830}$Vq$_{180}$MAA$_{1350}$ micelles, the preparation procedure was analogue to the one described above, but with adjusted amounts of material (31.45 mg B$_{830}$V$_{180}$T$_{1350}$ triblock terpolymer, 8 mL of Me$_2$SO$_4$, 0.28 g of Me$_2$SO$_4$, 1.89 g of conc. HCl and 5.48 mg of porphyrazine derivate). The micelle solutions which were not used for complex formation with PLL-b-PEG were filtered with 0.8 μm syringe filters and the polymer concentration was determined by weight from aliquots after dialysis to Milli-Q water and freeze-drying. PS concentration was determined from freeze-dried aliquots by redissolving the PS in DMAc and measuring the absorbance at 552 and 620 nm.

Preparation and Cross-Linking of BVqMAA/PLL-b-PEG. To BVqMAA micellar solutions in PBS buffer, PLL-b-PEG (or PDLL-b-PEG) was added from a stock solution (10 g/L in 10 mM PBS adjusted to pH 7.4 with additional 140 mM NaCl) and the complexes were allowed to form by shaking at room temperature for 7 d. The amount of added diblock copolymer was adjusted, so that $Z_{+/-}$-values of 0.25, 0.50, and 1 (see eq 1) compared to the residual MAA units after intramicellar complex formation (MAA − Vq units) were reached, thereby creating complex micelles with increasing degree of PEGylation. Subsequently, a 4-fold excess of EDC compared to the COOH groups of PMAA was directly dissolved in the mixture and was stirred for 12 h at room temperature, before dialysis against PBS buffer (10 mM at pH 7.4 with 140 mM NaCl) with a 6−8 kDa MWCO dialysis membrane for several days. PEGylated micelle solutions were then filtered with a 0.8 μm syringe filter and polymer and PS concentration was determined as described for the non-PEGylated BVqMAA micelles.

Characterization. *MALDI-ToF-MS.* Measurements were performed on a Bruker Daltonics Reflex III instrument equipped with an N$_2$ Laser (337 nm) and an acceleration voltage of 20 kV in positive ion mode. Sample preparation was done according to the "dried-droplet" method. In detail, matrix (DCTB, conc. 20 mg/mL), analyte (conc. 10 mg/mL) and salt (AgTFA, conc. 10 mg/mL) were separately dissolved in THF, subsequently mixed in a ratio of 20/5/1 μL. Approximately 1 μL of the final mixture was applied to the target spot and left to dry under air.

^{1}*H NMR.* Spectra of PB, PB-b-P2VP and PB-b-P2VP-b-PtBMA were recorded on a Bruker Ultrashield 300 machine with a 300 MHz operating frequency using deuterated chloroform (CDCl$_3$) as solvent. PLL(TFA)-b-PEG and PLL-b-PEG were measured using a 300 MHz spectrometer (EX 300, JEOL, Tokyo, Japan) with DMSO-d_8 and D$_2$O as solvents, respectively.

Potentiometric Titration. Micelle solutions (1 mL of 1 g/L in water containing 140 mM NaCl) were adjusted to low pH through addition of 0.5 M HCl before being titrated at ambient temperature and under stirring with 0.01 N NaOH solution, while monitoring the solution pH with a pH electrode.

Dynamic Light Scattering (DLS). The z-average hydrodynamic diameter, D_h, of the micelles was determined by cumulant analysis at ambient temperature using a Zetasizer Nano-ZS instrument (Malvern Instruments, Malvern, U.K.) equipped with a He−Ne ion laser $\lambda = 633$ nm and at a scattering angle of 173°. A low volume quartz cuvette (ZEN2112) was used for each measurement. For serum stability experiments, an ALV DLS/SLS-SP 5022F compact goniometer system with an ALV 5000/E cross correlator and a He−Ne laser ($\lambda = 632.8$ nm) was used. The measurements were carried out in cylindrical scattering cells ($d = 10$ mm) at an angle of 90° and 37 °C in triplicate on the same sample. The CONTIN algorithm was applied to analyze the obtained correlation functions. Apparent hydrodynamic radii were calculated according to the Stokes−Einstein equation.

ζ-Potential Measurements. Measurements were performed in triplicate on the same instrument used for DLS with disposable capillary cells (DTS1061), where approximately 800 μL of the micelle solution in PBS (10 mM PBS at pH 7.4 with additional 140 mM NaCl) was used per sample. The ζ-potential was calculated from was obtained electrophoretic mobility by applying the Smoluchowski equation.

Cryogenic Transmission Electron Microscopy (Cryo-TEM). For cryo-TEM studies, a drop (∼2 μL) of the aqueous micellar solution ($c \sim 0.5$ g L^{-1}) was placed on a lacey carbon-coated copper TEM grid (200 mesh, Science Services), where most of the liquid was removed with filter paper, leaving a thin film spread between the carbon coating. The specimens were shock vitrified by rapid immersion into liquid ethane in a temperature-controlled freezing unit (Zeiss Cryobox, Zeiss NTS GmbH) and cooled to approximately 90 K. The temperature was monitored and kept constant in the chamber during all of the preparation steps. After freezing the specimens they were inserted into a cryo-transfer holder (CT3500, Gatan) and transferred to a Zeiss EM922 OMEGA EFTEM instrument. Measurements were carried out at temperatures around 90 K. The microscope was operated at an acceleration voltage of 200 kV. Zero-loss filtered images ($\Delta E = 0$ eV) were taken under reduced dose conditions. All images were recorded digitally by a bottom mounted CCD camera system (Ultrascan 1000, Gatan), and processed with a digital imaging processing system (Gatan Digital Micrograph 3.9 for GMS 1.4).

Size Exclusion Chromatography (SEC). For the PB and PB-b-P2VP precursor polymers and BVT triblock terpolymers, a Waters instrument calibrated with narrowly distributed 1,4-PB standards at 40 °C and equipped with four PSS-SDV gel columns (5 μm particle size) with a porosity range from 10^2 to 10^5 Å (PSS, Mainz, Germany) was used together with a differential refractometer and a UV detector at 260 nm. Measurements were performed in THF with a flow rate of 1 mL/min using toluene as internal standard. For PEG-NH$_2$, PLL(TFA)-b-PEG and PDLL(TFA)-b-PEG polymers, a Tosoh instrument (Yamaguchi, Japan) calibrated with PEG standards and equipped with three TSK columns (TSKguardcolumn HHR-L; TSKgel G4000HHR; TSKgel G3000HHR) and a refractive index detector (RI) at 40 °C was used. DMF with 10 mM LiCl was used as eluent at a flow rate of 0.8 mL/min. Sample concentration was 1 mg/mL and 100 μL was injected per measurement.

Serum Stability Experiments. Micellar solutions (nondrug-carrying micelles Table S3) were prepared in Dulbecco's modified eagle medium (GIBCO) containing 10% fetal bovine serum (GIBCO) at a concentration of 0.2 mg/mL and incubated at 37 °C in a water bath. At the appropriate times, an aliquot (1 mL) was removed from the respective solution for light scattering measurement.

***In Vitro* Study.** *Cell Culturing Conditions.* A549 human lung adenocarcinoma cells were purchased from Riken cell bank (Tsukuba, Japan). A549 cells were cultured with Dulbecco's modified eagle medium (Sigma, Japan) containing 10% fetal bovine serum (GIBCO, Japan) and Penicillin/Streptomycin (Sigma, Japan) in a humidified atmosphere containing 5% CO$_2$ at 37 °C.

The passage of the cells was trypsinized with Trypsin-EDTA solution (Sigma, Japan) after being washed with D-PBS (Wako, Japan).

Cytotoxicity. A549 cells were seeded in 96-well plates at a density of 5000 cells/well in 50 μL of medium and incubated overnight. Then, 50 μL of medium containing the appropriate amount of polymer micelles were added to each well. The first row of 12 rows in each 96-well plate contained only medium but no cells and was used as a background, while the second row contained cells but was not treated with micelles to serve as reference for cell viability. Samples treated with micelles ($n = 4$) had a maximum concentration of 10 μg/mL with regard to the amount of PS, which decreased by a factor of 2 for each step in the concentration range. Non-PS-carrying-polymer micelles were tested at a maximum polymer concentration of 0.1 mg/mL. After incubating for 24 h, the plates were illuminated under a 300-W halogen lamp (fluence rate, 3.0 mW cm^{-2}) equipped with a band-pass filter (400−700 nm) for 0, 15, and 30 min, while being placed on a frozen refrigerant-filled 6-well plate for cooling. The medium was replaced with 100 μL of fresh medium per well after further incubating for 24 h. Then, 20 μL of MTT solution (5 mg/mL in PBS) was added to each well and the samples were incubated for further 3 h. Subsequently, 100 μL of SDS solution (20 wt %) was added to each well and the plates were incubated overnight, before the absorption at 570 nm was determined with a plate-reader. The mean absorption value of the background row was subtracted before further evaluation. Cell viability was determined relative to the control row of each plate.

Cellular Uptake. A549 cells were seeded in 6-well plates at a density of 1×10^6 cells/well in 2 mL of medium and incubated overnight before the medium was replaced by fresh DMEM containing micelles at 1 μg PS/mL (2 mL/well total volume). After 24 h incubation, the PS-containing medium was removed and each well was washed twice with cold PBS before 900 μL of SDS solution (20 wt %) was added. PS concentration was determined from the fluorescence signal at 627 nm (excitation at 400 nm) with a fluorophotometer after incubation overnight directly from SDS solutions. From a control plate, which had not been treated with the micelles, the cell number per well was determined by detaching the cells with trypsin solution and subsequent cell counting with a NucleoCounter NC-100 (Eppendorf AG, Hamburg, Germany). Measurements were performed in triplicate for each sample.

***In Vivo* Study.** *Breeding Information.* Five weeks-old female nude mice (Balb/c nu/nu mice: CAnN.Cg-*Foxn*^{1nu} /CrlCrlj) were purchased from Charles River Laboratories (Yokohama, Japan) *via* Oriental Yeast Co. Ltd. (Tokyo, Japan) and maintained under the standard conditions (20 °C, relative humidity, light/dark cycles) at our animal facilities in the University of Tokyo.

Blood Circulation Study. Blood circulation of the micelles was evaluated using intravital real-time confocal laser scanning microscopy (IVRTCLSM) in live mice. All images were acquired using a Nikon A1R confocal laser scanning microscope system attached to an upright ECLIPSE FN1 (Nikon Corp., Tokyo, Japan) equipped with a 20× objective (numerical aperture: 0.75), 561 nm laser, and a band-pass emission filter of 570−620 nm. Balb/c nu/nu mice were anesthetized with 2.0−3.0% isoflurane (Abbott Japan Co., Ltd., Tokyo, Japan) using a Univenter 400 anesthesia unit (Univentor Ltd., Zejtun, Malta). Mice were then subjected to lateral tail vein catheterization with a 30 gauge needle (Dentronics Co., Ltd., Tokyo, Japan) connected to a non-toxic, medical grade polyethylene tube (Natsume Seisakusho Co., Ltd., Tokyo, Japan). Anesthetized mice were placed onto a temperature-controlled pad (Thermoplate; Tokai Hit Co., Ltd., Shizuoka, Japan) integrated into the microscope stage and maintained in a sedated state throughout the measurement. Ear-lobe dermis was observed following fixation beneath a coverslip with a single drop of immersion oil. Data were acquired at 12 frames/min for 3 min, followed by snap-shots every 1 min thereafter. Micelles were injected (200 μL of the respective BVqMAA/PLL-*b*-PEG solution) *via* the tail vein 10 s after the start of video capture. Video data were analyzed by selecting regions of interest (ROIs) within blood vessels and the average fluorescence intensity per pixel for each time point was determined using the Nikon NIS-Elements C software (Nikon Corp.). *Relative fluorescence intensity* shown in Figure 4A,B was obtained with the following equation:

$$\begin{aligned} \text{relative fluorescence intensity} \\ = (\text{fluorescence intensity at indicated time point} \\ - \text{ initial fluorescence intensity})/ \\ (\text{maximum fluorescence intensity} \\ - \text{ initial fluorescence intensity}) \end{aligned}$$

Biodistribution Study. Balb/c nu/nu mice ($n = 24$) were inoculated subcutaneously with A549 cells (100 μL of 1×10^8 cells/mL). Tumors were allowed to grow for one week before the mice were separated into groups of 4. Then, polymer micelles with long- and short PMAA block and varying degree of PEGylation ($Z_{+/-} = 0$; 0.25, 0.50 and 1) were injected into the tail vein at 10 μg/mouse based on the PS (maximum injection volume was 190 μL). Twenty-four h post micelle injection, mice were sacrificed and kidneys, liver, spleen, lung and tumor were collected for the biodistribution study. The PS concentration of each sample was determined by fluorescence intensity at 627 nm in DCM (excitation at 400 nm) in a fluorophotometer after being extracted as follows: 250 μL and 1 mL of SDS solution (20 wt %) were added to 50 μL of the heavy blood components and for 200 mg of tissue, respectively, and the samples were sonicated until a homogeneous mixture was obtained. Then, the samples were shaken overnight at room temperature before 200 μL of DCM was added, followed by a short sonication step. Plasma samples of 40 μL were mixed with 200 μL of DCM, shaken at room temperature overnight, before being shortly sonicated with a sonication finger. All samples were then centrifuged at 10 000g for 30 min to induce phase separation before measurement of the DCM phase.

Tumor Suppression Study. Balb/c nu/nu mice ($n = 25$) were inoculated subcutaneously with A549 cells (100 μL of 1×10^8 cells/mL). Tumors were allowed to grow for 10 days until they reach approximately 25 mm^3. Mice were separated in groups of 5. Then, non-PEGylated micelles and PEGylated micelles at 30 μg/kg based on PS were intravenously injected. Twenty-four hours later, mice were irradiated at the tumor position for 1000 s at 100 mW/cm^2 by using a Xenon lamp with a 630 nm long-path filter (Asahi Spectra, Tokyo, Japan). Mice in control groups were not irradiated. The antitumor activity was evaluated in terms of tumor size (V), as estimated by the following equation:

$$V = a \times b^2/2$$

where a and b are the major and minor axes of the tumor measured by a caliper, respectively. The body weight was measured simultaneously and was taken as a parameter of systemic toxicity. The statistical analysis of animal data was carried out by the unpaired Student's t test. All animal experiments were performed following the guidelines of the ethical committee of the University of Tokyo.

Conflict of Interest: The authors declare no competing financial interest.

Supporting Information Available: Molecular characterization of the polymer samples as well as physical and biological characterization of BVqMAA/PLL-*b*-PEG and BVqMAA/PDLL-*b*-PEG micelles is provided. This material is available free of charge *via* the Internet at http://pubs.acs.org.

REFERENCES AND NOTES

1. Ariga, K.; Ji, Q.; McShane, M. J.; Lvov, Y. M.; Vinu, A.; Hill, J. P. Inorganic Nanoarchitectonics for Biological Applications. *Chem. Mater.* **2012**, *24*, 728–737.

2. Goldberg, M.; Langer, R.; Jia, X. Nanostructured Materials for Applications in Drug Delivery and Tissue Engineering. *J. Biomater. Sci., Polym. Ed.* **2007**, *18*, 241–268.

3. Petkar, K. C.; Chavhan, S. S.; Agatonovik-Kustrin, S.; Sawant, K. K. Nanostructured Materials in Drug and Gene Delivery: A Review of the State of the Art. *Crit. Rev. Ther. Drug Carrier Syst.* **2011**, *28*, 101–164.

4. Shanmugam, T.; Banerjee, R. Nanostructured Self Assembled Lipid Materials for Drug Delivery and Tissue Engineering. *Ther. Delivery* **2011**, *2*, 1485–1516.

5. Tang, Z.; Wang, Y.; Podsiadlo, P.; Kotov, N. A. Biomedical Applications of Layer-by-Layer Assembly: From Biomimetics to Tissue Engineering. *Adv. Mater.* **2006**, *18*, 3203–3224.

6. Cabral, H.; Kataoka, K. Multifunctional Nanoassemblies of Block Copolymers for Future Cancer Therapy. *Sci. Technol. Adv. Mater.* **2010**, *11*, 014109.

7. Kataoka, K.; Harada, A.; Nagasaki, Y. Block Copolymer Micelles for Drug Delivery: Design, Characterization and Biological Significance. *Adv. Drug Delivery Rev.* **2001**, *47*, 113–131.

8. Miyata, K.; Christie, R. J.; Kataoka, K. Polymeric Micelles for Nano-Scale Drug Delivery. *React. Funct. Polym.* **2011**, *71*, 227–234.

9. Savic, R.; Eisenberg, A.; Maysinger, D. Block Copolymer Micelles as Delivery Vehicles of Hydrophobic Drugs: Micelle-Cell Interactions. *J. Drug Targeting* **2006**, *14*, 343–355.

10. Kelkar, S. S.; Reineke, T. M. Theranostics: Combining Imaging and Therapy. *Bioconjugate Chem.* **2011**, *22*, 1879–1903.

11. Kim, J.; Piao, Y.; Hyeon, T. Multifunctional Nanostructured Materials for Multimodal Imaging, and Simultaneous Imaging and Therapy. *Chem. Soc. Rev.* **2009**, *38*, 372–390.

12. Nyström, A. M.; Wooley, K. L. The Importance of Chemistry in Creating Well-Defined Nanoscopic Embedded Therapeutics: Devices Capable of the Dual Functions of Imaging and Therapy. *Acc. Chem. Res.* **2011**, *44*, 969–978.

13. Cabral, H.; Nishiyama, N.; Kataoka, K. Supramolecular Nanodevices: From Design Validation to Theranostic Nanomedicine. *Acc. Chem. Res.* **2011**, *44*, 999–1008.

14. Elsabahy, M.; Wooley, K. L. Strategies Toward Well-Defined Polymer Nanoparticles Inspired by Nature: Chemistry *versus* Versatility. *J. Polym. Sci., Part A: Polym. Chem.* **2012**, *50*, 1869–1880.

15. Moughton, A. O.; Hillmyer, M. A.; Lodge, T. P. Multicompartment Block Polymer Micelles. *Macromolecules* **2012**, *45*, 2–19.

16. Synatschke, C. V.; Schacher, F. H.; Förtsch, M.; Drechsler, M.; Müller, A. H. E. Double-Layered Micellar Interpolyelectrolyte Complexes - How Many Shells to a Core? *Soft Matter* **2011**, *7*, 1714–1725.

17. Bastakoti, B. P.; Wu, K. C. W.; Inoue, M.; Yusa, S.-I.; Nakashima, K.; Yamauchi, Y. Multifunctional Core-Shell-Corona-Type Polymeric Micelles for Anticancer Drug-Delivery and Imaging. *Chem.—Eur. J.* **2013**, *19*, 4812–4817.

18. Koo, H.; Huh, M. S.; Sun, I.-C.; Yuk, S. H.; Choi, K.; Kim, K.; Kwon, I. C. *In Vivo* Targeted Delivery of Nanoparticles for Theranosis. *Acc. Chem. Res.* **2011**, *44*, 1018–1028.

19. Petros, R. A.; DeSimone, J. M. Strategies in the Design of Nanoparticles for Therapeutic Applications. *Nat. Rev. Drug Discovery* **2010**, *9*, 615–627.

20. Dolmans, D.; Fukumura, D.; Jain, R. K. Photodynamic Therapy for Cancer. *Nat. Rev. Cancer* **2003**, *3*, 380–387.

21. Henderson, B. W.; Dougherty, T. J. How Does Photodynamic Therapy Work? *Photochem. Photobiol.* **1992**, *55*, 145–157.

22. O'Connor, A. E.; Gallagher, W. M.; Byrne, A. T. Porphyrin and Nonporphyrin Photosensitizers in Oncology: Preclinical and Clinical Advances in Photodynamic Therapy. *Photochem. Photobiol.* **2009**, *85*, 1053–1074.

23. Palumbo, G. Photodynamic Therapy and Cancer: A Brief Sightseeing Tour. *Expert Opin. Drug Delivery* **2007**, *4*, 131–148.

24. Schacher, F.; Walther, A.; Müller, A. H. E. Dynamic Multicompartment-Core Micelles in Aqueous Media. *Langmuir* **2009**, *25*, 10962–10969.

25. Schacher, F.; Betthausen, E.; Walther, A.; Schmalz, H.; Pergushov, D. V.; Müller, A. H. E. Interpolyelectrolyte Complexes of Dynamic Multicompartment Micelles. *ACS Nano* **2009**, *3*, 2095–2102.

26. Borisov, O.; Zhulina, E.; Leermakers, F.; Ballauff, M.; Müller, A. H. E. In *Self Organized Nanostructures of Amphiphilic Block Copolymers I*; Müller, A. H. E.; Borisov, O., Eds.; Springer: Berlin/Heidelberg, 2011; pp 1−55.

27. Townend, R.; Kumosinski, T. F.; Timasheff, S. N.; Fasman, G. D.; Davidson, B. The Circular Dichroism of the β Structure of Poly-L-Lysine. *Biochem. Biophys. Res. Commun.* **1966**, *23*, 163–169.

28. Pergushov, D. V.; Müller, A. H. E.; Schacher, F. H. Micellar Interpolyelectrolyte Complexes. *Chem. Soc. Rev.* **2012**, *41*, 6888–6901.

29. Morgan, A. R.; Petousis, N. H.; van Lier, J. E. Synthesis and Photodynamic Activity of Some Tetraazoporphyrin Derivatives. *Eur. J. Med. Chem.* **1997**, *32*, 21–26.

30. Tonga, G. Y.; Saha, K.; Rotello, V. M. 25th Anniversary Article: Interfacing Nanoparticles and Biology: New Strategies for Biomedicine. *Adv. Mater.* **2013**, 10.1002/adma.201303001.

31. Maeda, H.; Wu, J.; Sawa, T.; Matsumura, Y.; Hori, K. Tumor Vascular Permeability and the EPR Effect in Macromolecular Therapeutics: A Review. *J. Controlled Release* **2000**, *65*, 271–284.

32. Matsumoto, Y.; Nomoto, T.; Cabral, H.; Matsumoto, Y.; Watanabe, S.; Christie, R. J.; Miyata, K.; Oba, M.; Ogura, T.; Yamasaki, Y.; *et al.* Direct and Instantaneous Observation of Intravenously Injected Substances Using Intravital Confocal Micro-Videography. *Biomed. Opt. Express* **2010**, *1*, 1209–1216.

33. Owens, D. E., III; Peppas, N. A. Opsonization, Biodistribution, and Pharmacokinetics of Polymeric Nanoparticles. *Int. J. Pharm.* **2006**, *307*, 93–102.

34. Tockary, T. A.; Osada, K.; Chen, Q.; Machitani, K.; Dirisala, A.; Uchida, S.; Nomoto, T.; Toh, K.; Matsumoto, Y.; Itaka, K.; *et al.* Tethered PEG Crowdedness Determining Shape and Blood Circulation Profile of Polyplex Micelle Gene Carriers. *Macromolecules* **2013**, *46*, 6585–6592.

35. Anraku, Y.; Kishimura, A.; Kobayashi, A.; Oba, M.; Kataoka, K. Size-Controlled Long-Circulating PICsome as a Ruler to Measure Critical Cut-Off Disposition Size into Normal and Tumor Tissues. *Chem. Commun.* **2011**, *47*, 6054–6056.

36. Brinkhuis, R. P.; Stojanov, K.; Laverman, P.; Eilander, J.; Zuhorn, I. S.; Rutjes, F. P. J. T.; van Hest, J. C. M. Size Dependent Biodistribution and SPECT Imaging of 111In-Labeled Polymersomes. *Bioconjugate Chem.* **2012**, *23*, 958–965.

37. Cho, W.-S.; Cho, M.; Jeong, J.; Choi, M.; Han, B. S.; Shin, H.-S.; Hong, J.; Chung, B. H.; Jeong, J.; Cho, M.-H. Size-Dependent Tissue Kinetics of PEG-Coated Gold Nanoparticles. *Toxicol. Appl. Pharmacol.* **2010**, *245*, 116–123.

38. Johnston, A. P. R.; Such, G. K.; Ng, S. L.; Caruso, F. Challenges Facing Colloidal Delivery Systems: From Synthesis to the Clinic. *Curr. Opin. Colloid Interface Sci.* **2011**, *16*, 171–181.

39. Fasman, G. D.; Idelson, M.; Blout, E. R. Synthesis and Conformation of High Molecular Weight Poly-Epsilon-carbobenzyloxy-L-lysine and Poly-L-lysine·HCl. *J. Am. Chem. Soc.* **1961**, *83*, 709–712.

40. Schacher, F.; Yuan, J.; Schoberth, H. G.; Müller, A. H. E. Synthesis, Characterization, and Bulk Crosslinking of Polybutadiene-*block*-Poly(2-vinyl pyridine)-*block*-Poly(*tert*-butyl methacrylate) Block Terpolymers. *Polymer* **2010**, *51*, 2021–2032.

41. Sperschneider, A.; Schacher, F.; Gawenda, M.; Tsarkova, L.; Müller, A. H. E.; Ulbricht, M.; Krausch, G.; Köhler, J. Towards Nanoporous Membranes Based on ABC Triblock Terpolymers. *Small* **2007**, *3*, 1056–1063.

42. Stadler, R.; Auschra, C.; Beckmann, J.; Krappe, U.; Voight-Martin, I.; Leibler, L. Morphology and Thermodynamics of Symmetric Poly(A-*block*-B-*block*-C) Triblock Copolymers. *Macromolecules* **1995**, *28*, 3080–3097.